Available online at www.sciencedirect.com
ScienceDirect
Thermochimica Acta 460 (2007) 53–59
thermochimica acta
www.elsevier.com/locate/tca

Kinetic study of a thermal dechlorination and oxidation of neodymium oxychloride

H.C. Yang [a,*], Y.J. Cho [a], H.C. Eun [b], E.H. Kim [a], I.T. Kim [a]

[a] *Advanced Fuel Cycle Development Group, Korea Atomic Energy Research Institute, P.O. Box 150, Yuseong, Daejeon 305-353, Republic of Korea*
[b] *Quantum Energy Chemical Engineering, University of Science and Technology, P.O. Box 52, Yuseong, Daejeon 305-333, Republic of Korea*

Received 26 February 2007; received in revised form 17 May 2007; accepted 24 May 2007
Available online 31 May 2007

Abstract

This study investigated the kinetics of a thermal dechlorination and oxidation of neodymium oxychloride (NdOCl) by using a non-isothermal thermogravimetric (TG) analysis under various oxygen partial pressures. The results of the isoconversional analysis of the TG data suggests that the dechlorination and oxidation of NdOCl follows a single step reaction and the observed activation energy was determined as $228.3 \pm 6.1\,\mathrm{kJ\,mol^{-1}}$. A kinetic rate equation was derived for a conversion of the NdOCl into Nd_2O_3 with a power law model, $f(\alpha) = 2/3\alpha^{-1/2}$. The oxygen power dependency and the pre-exponential factor were determined as 0.315 and $3.55 \times 10^5\,\mathrm{s^{-1}\,Pa^{-0.315}}$, respectively.

Keywords: Non-isothermal thermogravimetric analysis; Thermal dechlorination; Oxidation; Neodymium oxychloride; Three-dimensional phase boundary reaction model

1. Introduction

Neodymium oxide, also called neodymia, has been widely used in photonic applications [1]. Glass containing neodymium oxide is used in astronomical work to produce sharp bands by which spectral lines may be calibrated. Neodymium oxides are also used as a laser material in place of ruby to produce a coherent light and as components of advanced materials such as high temperature ceramics and superconductors and of catalytic systems [2–4].

Neodymium oxides have usually been prepared by a well known chemical synthesis process with alkoxides as precursors. There are, however, some difficulties in the synthesis of rare earth alkoxides [1]. An electrochemical separation and an electrochemical synthesis in molten chloride salts are promising technologies for obtaining pure metals and oxides of rare earth (RE) [5–8]. By-products of these electrochemical processes include RE oxychlorides (REOCl) such as neodymium oxychloride (NdOCl). Pure Nd oxides are additionally obtained by a thermal treatment of the Nd oxychlorides to emit gaseous chlorines in the presence of oxygen as:

$$2\mathrm{NdOCl} + (1/2)\mathrm{O_2(g)} = \mathrm{Nd_2O_3} + \mathrm{Cl_2(g)}$$

Detailed kinetics of the above dechlorination and oxidation reaction of NdOCl have not been reported in the existing literatures as yet.

TG methods, such as isothermal and non-isothermal methods have been used widely to establish the kinetics for a conversion of many solids [9–12]. A non-isothermal TG study has an advantage in that a wide range of temperatures are covered with a single experiment. This study investigated the kinetics of a thermal dechlorination and oxidation of NdOCl by using a non-isothermal thermogravimetric (TG) analysis under various oxygen partial pressures. The objectives of this study were to establish a detailed kinetic model and the kinetic parameters of the dechlorination and oxidation reaction of NdOCl under high-temperature oxidizing atmospheres.

2. Theoretical

The influence of the temperature and that of an oxygen partial pressure on the dechlorination and oxidation reaction for NdOCl can be described with an Arrhenius equation and a power law

* Corresponding author. Tel.: +82 42 868 2575; fax: +82 42 868 2329.
E-mail address: nhcyang@kaeri.re.kr (H.C. Yang).

0040-6031/$ – see front matter © 2007 Elsevier B.V. All rights reserved.
doi:10.1016/j.tca.2007.05.019

approach, respectively. The reaction rate is thus described as:

$$\frac{d\alpha}{dt} = k_0(P_{O_2})^n \exp\left(-\frac{E}{RT}\right) f(\alpha) \quad (1)$$

where α is the extent of a conversion, k_0 the reaction rate constant ($s^{-1}\,Pa^{-n}$), P_{O_2} the oxygen partial pressure (Pa) and n is the power dependency of the oxygen partial pressure. The function $f(\alpha)$ represents the influence of a conversion on the conversion rate. In the case of a non-isothermal reaction, the applied heating rates are constant and the temperature can be expressed as $T = Bt = T_0$ in which the constant heating rate, B, is given as $dT/dt = B$. Using this transformation of Eq. (1) and a separation of the variables results in:

$$\frac{d\alpha}{f(\alpha)} = \frac{k_0}{B}(P_{O_2})^n \exp\left(-\frac{E}{RT}\right) dT \quad (2)$$

which can be rewritten as

$$g(\alpha) = \frac{ZE}{BR} p(y) \quad (3)$$

in which $g(\alpha)$ is the result of an integral on the left hand side of Eq. (2), $Z = k_0(P_{O_2})^n$, and $p(y)$ is a function of the temperature integral on the right hand side of Eq. (2):

$$p(y) = \int_{y_0}^{y_c} \frac{e^{-y}}{y^2} dy = \frac{e^{-y}}{y^2} + \int_{y_0}^{y_c} \frac{e^{-y}}{y} dy \quad (4)$$

in which $y = -E/RT$. The kinetic parameters Z and E in Eq. (3) are invariable for a single step reaction. By using a reference at a half conversion ($\alpha = 0.5$), Eq. (3) is converted into

$$g(0.5) = \frac{ZE}{BR} p(y_{0.5}) \quad (5)$$

where $y_{0.5} = E/RT_{(0.5)}$. Dividing Eq. (3) by Eq. (5), the following equation is given.

$$\frac{g(\alpha)}{g(0.5)} = \frac{p(y)}{p(y_{0.5})} \quad (6)$$

Theoretical master plots are given by plotting $g(\alpha)/g_{(0.5)}$ for various $g(\alpha)$ functions. In order to obtain experimental master plots of $p(y)/p(y_{0.5})$ against a conversion α from the experimental data, the temperature as a function of α and E should be established in advance. Eq. (4) is not analytically solvable and many approximations have been proposed and they are still being discussed [13–16]. An accurate approximate formula for $p(y)$ proposed by Wanjun et al. [16] is applied in the present study.

$$-\ln[p(y)] = 0.377739 + 1.894661 \ln y + 1.001450 y \quad (7)$$

By introducing Eq. (7) into Eq. (3), Eq. (8) is obtained.

$$\ln\left(\frac{B}{T^{1.894661}}\right) = \ln\left(\frac{ZE}{Rg(\alpha)}\right) + 3.635041 - 1.894661 \ln E - 1.001450\left(\frac{E}{RT}\right) \quad (8)$$

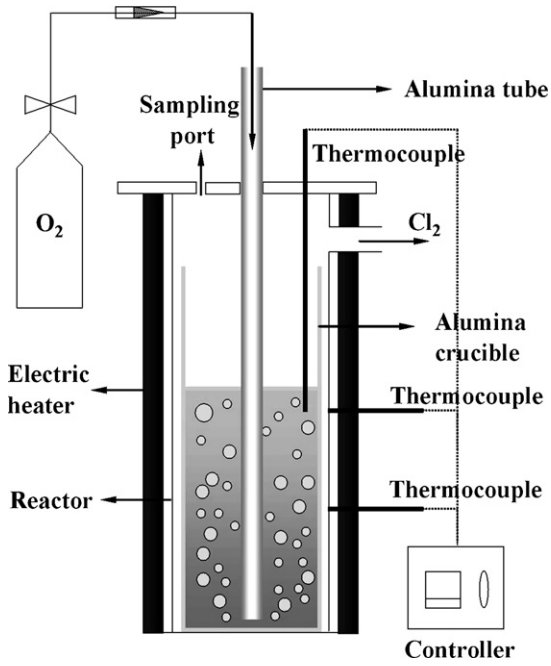

Fig. 1. A schematic experimental apparatus for synthesizing the NdOCl.

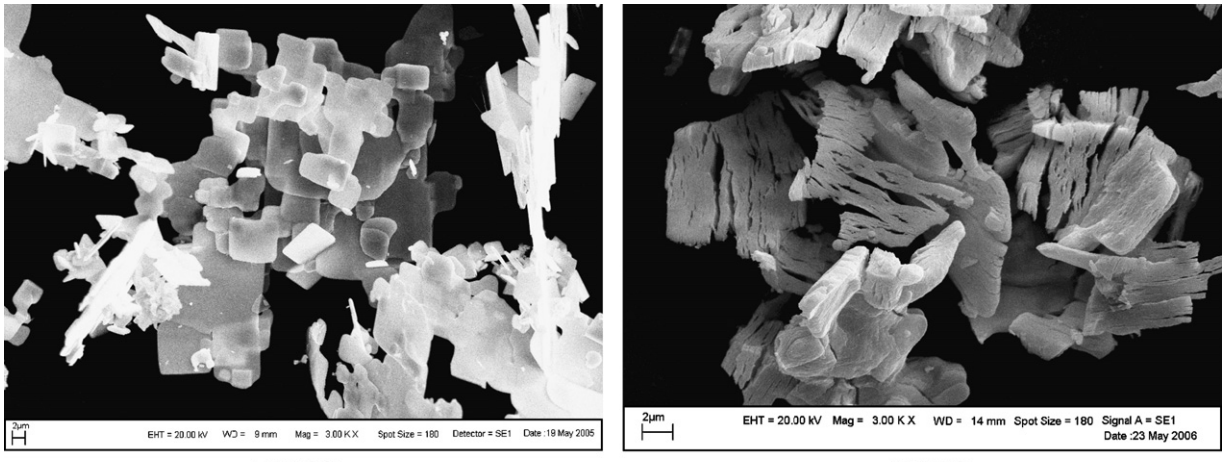

(a) NdOC1 (b) Nd_2O_3

Fig. 2. SEM photograph of synthesized NdOCl (a) and its post-TG product, Nd_2O_3 (b).

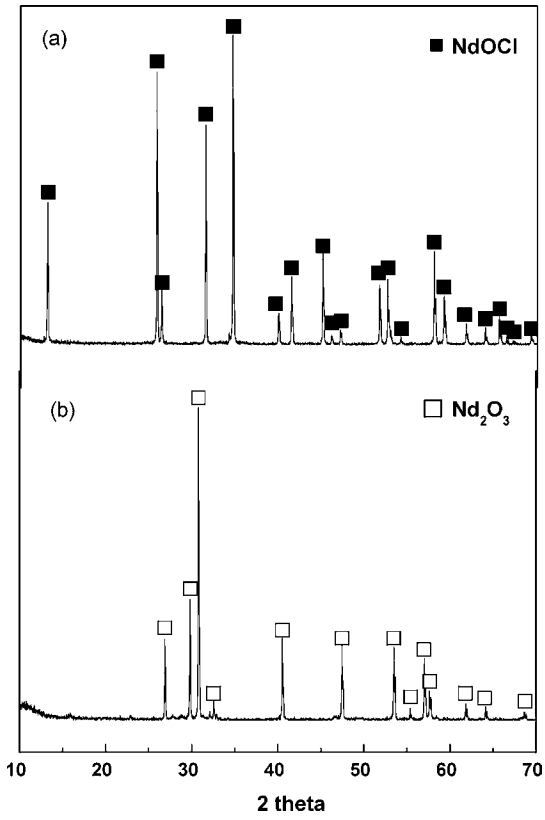

Fig. 3. Powdered XRD patterns of synthesized NdOCl (a) and its post-TG product, Nd_2O_3 (b).

Assuming that neither the reaction model, $g(\alpha)$, nor the activation energy, E, change for all the conversion levels under a constant oxygen partial pressure, a plot of $\ln(B/T^{1.894661})$ against the reciprocal of the absolute temperature ($1/T$) at any given value of α should lead to the same slopes according to Eq. (8), which provide the activation energy of the reaction:

$$E = \frac{-R}{1.001450}\left(\frac{\mathrm{d}\ln(B/T^{1.894661})}{\mathrm{d}(1/T)}\right) \quad (9)$$

Once the activation energies have been determined, an appropriate kinetic model can be found by a comparison of the experimental master plots with the theoretical master plots for various reaction models. Based on the determined activation energy E and conversion model $g(\alpha)$, the Z values, which are different for each oxygen partial pressure, are determined by the logarithms of Eq. (3).

$$\ln[p(y)] = \ln(B) - \ln\left(\frac{ZE}{R}\right) + \ln(g(\alpha)) \quad (10)$$

The reaction order with respect to the oxygen partial pressure, n, is estimated from the slope of a graph for the logarithmic of Z versus the logarithmic of the oxygen partial pressure (P_{O_2}).

$$\ln Z = \ln k_0 + n \ln P_{O_2} \quad (11)$$

3. Experimental methods

3.1. Synthesis and analysis of NdOCl and its thermal oxidation products

Powdered NdOCl was synthesized in LiCl–KCl eutectic molten salt. The experimental apparatus for synthesizing the NdOCl is shown in Fig. 1. Anhydrous $NdCl_3$ with a purity of 99.99% was premixed with a LiCl–KCl solid salt with a purity of 99.9% (LiCl: 44.2 wt.%, eutectic point: 633 K) in an alumina crucible. The crucible containing the mixture was heated up to 723 K in a stainless-steel column and oxygen was sparged into it from the bottom. After a 7-h oxygen sparging, the mixture of the precipitate was sampled and dissolved in distilled water. A pure sample powder of NdOCl, was then obtained by a vacuum filtration. SEM photographs of the obtained NdOCl powder and its thermal oxidation product, Nd_2O_3 powder, are shown in Fig. 2. Speciation of the obtained samples before and after a thermal oxidation was performed by a powdered XRD pattern analysis and the results are shown in Fig. 3.

3.2. TG analysis

Non-isothermal TG analyses by using TG/DTA (SDT-6120, TA instruments Inc.) were performed from room temperature to 1673 K. The temperature of the furnace was programmed

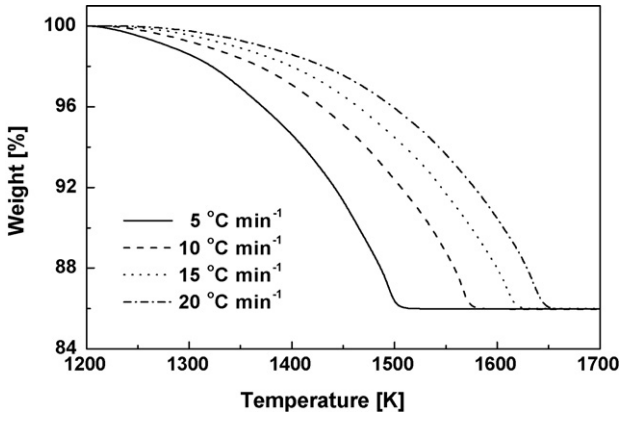

Fig. 4. Typical mass loss patterns of NdOCl at various heating rates under a fixed oxygen partial pressure ($P_{O_2} = 50$ kPa).

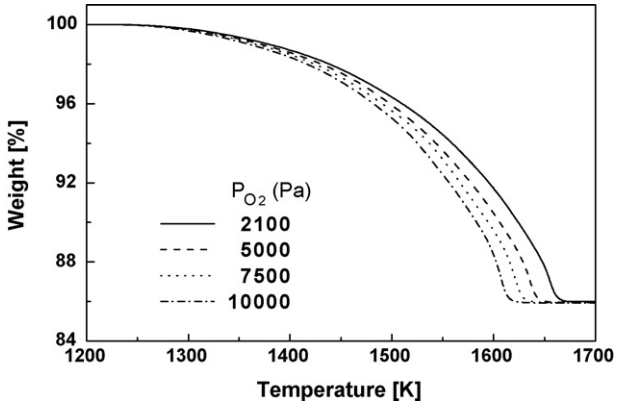

Fig. 5. Typical mass loss patterns of NdOCl at a fixed heating rate (5 °C min^{-1}) under various O_2 partial pressures.

to rise from room temperature to 1073 K with a heating rate of 50 K min^{-1}. After an initial rapid heating, the furnace was slowly heated from 1073 K to 1673 K with heating rates of 5, 10, 15 and 20 K min^{-1}. At each heating rate condition, four oxygen partial pressures were tested: 21, 50, 75 and 100 kPa of oxygen and the remainder consisted of pure nitrogen (>99.9%).

4. Results and discussion

4.1. Mass change patterns of the NdOCl

The mass loss as a function of the temperature of the NdOCl powders at different heating rates under a fixed O_2 condition and those at a fixed heating rate under different O_2 conditions are plotted in Figs. 4 and 5, respectively. Increasing the heating rate or decreasing the gaseous oxygen concentration resulted in a decrease in the conversion rate. This indicates that the conversion of NdOCl into Nd_2O_3 is an oxygen-dependent endothermic reaction.

4.2. Activation energy estimation

Obtained thermo-gravimetric data was analyzed to determine the activation energy for different levels of a conversion by using Eq. (9). A typical plot, constructed to evaluate the slopes $d\ln(B/T^{1.894661})/d(1/T)$, is shown in Fig. 6. If the conversion mechanisms are the same at all the conversion levels, the lines would all have the same slopes, which is the case here. This process was repeated for different sets of experiments at different partial pressures of oxygen. Determined activation energies for all the different conditions are plotted in Fig. 7. It was observed from Fig. 7 that the activation energy was not really changed and nearly independent with respect to the level of a conversion. This suggests that the dechlorination and oxidation of NdOCl follows a single step reaction. The activation energy were determined as 228.3 ± 6.1 kJ mol^{-1}. It should be noted that these results were obtained without any knowledge of the reaction model $f(\alpha)$.

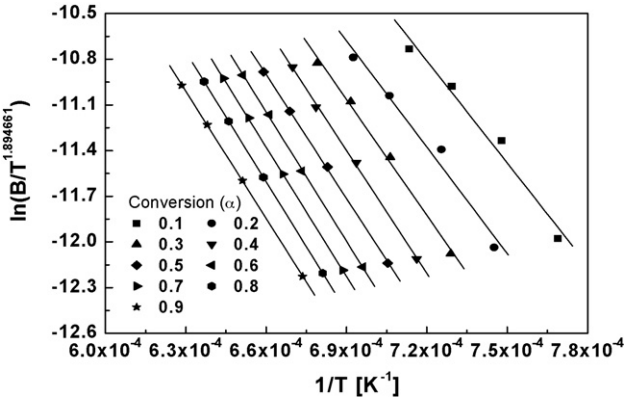

Fig. 6. Typical isoconversional plots for the determination of an activation energy of the dechlorination and oxidation of NdOCl ($P_{O_2} = 50$ kPa).

4.3. Kinetic model determination

Following the evaluation of the activation energy, the conversion model was determined by means of master-plots methods

Table 1
Kinetic model equations examined in this study

No.	Symbol	Reaction model	$f(\alpha)$	$g(\alpha)$
Avarmi–Erofeev				
1	A1/2	$n = 0.5$	$(1/2)\,(1-\alpha)[-\ln(1-\alpha)]^{-1}$	$[-\ln(1-\alpha)]^2$
2	A3/2	$n = 1.5$	$(3/2)\,(1-\alpha)[-\ln(1-\alpha)]^{1/3}$	$[-\ln(1-\alpha)]^{2/3}$
3	A2	$n = 2$	$2(1-\alpha)[-\ln(1-\alpha)]^{1/2}$	$[-\ln(1-\alpha)]^{1/2}$
4	A3	$n = 3$	$3(1-\alpha)[-\ln(1-\alpha)]^{2/3}$	$[-\ln(1-\alpha)]^{1/3}$
5	A4	$n = 4$	$4(1-\alpha)[-\ln(1-\alpha)]^{3/4}$	$[-\ln(1-\alpha)]^{1/4}$
Phase boundary controlled reaction				
6	R1	Contracting linear	1	α
7	R2	Contracting area	$2(1-\alpha)^{1/2}$	$1-(1-\alpha)^{1/2}$
8	R3	Contracting volume	$3(1-\alpha)^{2/3}$	$1-(1-\alpha)^{1/3}$
Diffusion				
9	D1	One-dimensional	$(1/2)\alpha$	α^2
10	D2	Two-dimensional	$1/[-\ln(1-\alpha)]$	$(1-\alpha)\ln(1-\alpha)+\alpha$
11	D3	Three-dimensional	$3(1-\alpha)^{1/3}/2[(1-\alpha)^{-1/3}-1]$	$[1-(1-\alpha)^{1/3}]^2$
12	D4	Jander equation	$(3/2)[(1-\alpha)^{-1/3}-1]$	$(1–2\alpha/3)-(1-\alpha)^{2/3}$
Power law				
13	P1	$n = 1/4$	$4\alpha^{3/4}$	$\alpha^{1/4}$
14	P2	$n = 1/3$	$3\alpha^{2/3}$	$\alpha^{1/3}$
15	P3	$n = 1/2$	$2\alpha^{1/2}$	$\alpha^{1/2}$
16	P4	$n = 3/2$	$2/3\alpha^{-1/2}$	$\alpha^{3/2}$
Chemical reaction				
17	F1	First order	$1-\alpha$	$-\ln(1-\alpha)$
18	F3/2	Three-halves order	$(1-\alpha)^{2/3}$	$2[(1-\alpha)^{-1/2}-1]$
19	F2	Second order	$(1-\alpha)^2$	$(1-\alpha)^{-1}-1$
20	F3	Third order	$(1-\alpha)^3$	$(1/2)[(1-\alpha)^{-2}-1]$

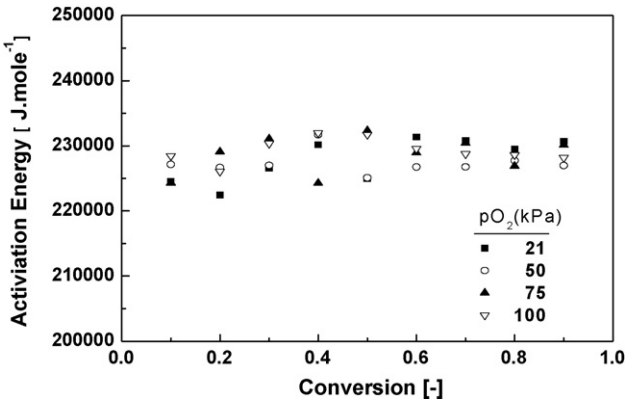

Fig. 7. Determined activation energy of the dechlorination and oxidation of NdOCl under different oxygen partial pressures, as a function of conversion.

[17]. By using the determined value of the activation energy E as a function of α for all the different conditions, the experimental master plots were constructed according to Eq. (4) as shown in Fig. 8. The theoretical master plots of the various kinetic functions listed in Table 1 are also plotted as solid lines in Fig. 8. The plots related to different heating rates under various oxygen partial pressures are practically identical. The comparison of the experimental master plots with the theoretical ones indicates that none of the existing theoretical master plots matched the experimental ones perfectly. However, the R3 and P4 models appear to be appropriate models for describing the reaction of a NdOCl dechlorination and oxidation. Several methods for a statistical justification of the selected models have been described by Vyazovkin and Wight [18]. In this study, a similar method was used to choose an acceptable model. An acceptable kinetic model for a NdOCl dechlorination and oxidation was selected based on the standard deviation (S.D.) between the theoretical master data and the experimental ones. The criterion for selecting an acceptable model can be taken as a sum of the S.D. as shown in Eq. (12) [19].

$$\sum \text{S.D.} = \sqrt{\frac{\sum_j^n \sum_i^m \left[g_k(\alpha_i)/g_k(0.5) - p_j(y_i)/p_j(y_{0.5})\right]^2}{(n-1)(m-1)}} \tag{12}$$

where m and n are the numbers of points and heating rates, respectively. The value of S.D. is the averaged square of the deviation between $p(y)/p(y_{0.5})$ calculated on the base of the experiment and $g_k(\alpha)/g_k(0.5)$, in which k denotes the serial number of the model functions listed in Table 1. If a model describes the experimental results accurately, it is possible to find a minimum for $\sum$S.D. The values of $\sum$S.D. for all different test conditions are listed in Table 2, in which model 16 revealed the minimum for $\sum$S.D. This comparison of the experimental master plots with the theoretical ones indicates that the mechanisms for a conversion of NdOCl into Nd_2O_3 could probably be described by a power low model P4 ($g(\alpha) = \alpha^{3/2}$). Therefore, the corresponding model equation for describing the conversion of NdOCl into Nd_2O_3 is given by:

$$g(\alpha) = \alpha^{3/2} = k_0 \exp\left(-\frac{E}{RT}\right)(P_{O_2})^n t \tag{13}$$

Table 2
Sum of the standard deviation (ΣS.D.) between the theoretical master data and the experimental ones

O_2 partial pressure (kPa)	Heating rate (K min^{-1})	Model[a]																			
		1	2	3	4	5	6	7	8	9	10	11	12	13	14	15	16	17	18	19	20
21	5	3.057	0.227	0.391	0.542	0.613	0.342	0.140	0.072	0.285	0.708	0.619	0.948	0.692	0.653	0.576	0.068	0.257	0.930	2.239	10.342
	10	2.997	0.297	0.461	0.610	0.681	0.413	0.212	0.133	0.217	0.641	0.685	0.883	0.760	0.721	0.645	0.139	0.213	0.875	2.184	10.279
	15	3.005	0.276	0.443	0.593	0.664	0.395	0.191	0.107	0.231	0.654	0.669	0.895	0.744	0.705	0.629	0.121	0.211	0.880	2.189	10.294
	20	3.116	0.191	0.346	0.496	0.567	0.289	0.102	0.087	0.340	0.764	0.573	1.005	0.645	0.604	0.526	0.022	0.316	0.990	2.299	10.402
50	5	3.082	0.200	0.364	0.514	0.586	0.314	0.113	0.059	0.313	0.734	0.591	0.974	0.664	0.625	0.548	0.046	0.280	0.954	2.263	10.365
	10	3.024	0.269	0.432	0.581	0.652	0.383	0.184	0.110	0.246	0.669	0.656	0.911	0.731	0.692	0.616	0.111	0.234	0.900	2.210	10.317
	15	3.033	0.248	0.413	0.564	0.635	0.366	0.162	0.083	0.261	0.683	0.640	0.923	0.715	0.675	0.599	0.092	0.234	0.906	2.215	10.320
	20	3.144	0.167	0.318	0.467	0.538	0.260	0.079	0.095	0.369	0.793	0.545	1.034	0.616	0.575	0.497	0.027	0.341	1.016	2.325	10.427
75	5	3.092	0.191	0.354	0.505	0.576	0.304	0.103	0.059	0.323	0.745	0.582	0.985	0.655	0.615	0.538	0.037	0.289	0.964	2.272	10.373
	10	3.039	0.255	0.417	0.566	0.637	0.368	0.169	0.100	0.261	0.685	0.642	0.926	0.716	0.677	0.601	0.097	0.246	0.914	2.224	10.330
	15	3.050	0.232	0.397	0.548	0.619	0.348	0.145	0.071	0.278	0.700	0.624	0.941	0.698	0.658	0.582	0.075	0.249	0.922	2.232	10.335
	20	3.162	0.153	0.300	0.449	0.520	0.240	0.069	0.107	0.389	0.812	0.527	1.053	0.598	0.557	0.478	0.043	0.359	1.034	2.343	10.444
100	5	3.100	0.184	0.345	0.496	0.567	0.296	0.096	0.060	0.331	0.753	0.573	0.993	0.646	0.606	0.530	0.033	0.297	0.972	2.281	10.382
	10	3.039	0.225	0.330	0.433	0.482	0.254	0.153	0.114	0.157	0.351	0.488	0.453	0.534	0.495	0.432	0.085	0.081	0.870	1.040	23.041
	15	3.050	0.232	0.397	0.548	0.619	0.348	0.145	0.071	0.278	0.700	0.624	0.941	0.698	0.658	0.582	0.075	0.249	0.922	2.232	10.335
	20	3.162	0.153	0.300	0.449	0.520	0.240	0.069	0.107	0.389	0.812	0.527	1.053	0.598	0.557	0.478	0.043	0.359	1.034	2.343	10.444
Total ΣS.D.	49.153	3.500	6.007	8.361	9.477	5.161	2.133	1.435	4.668	11.204	9.563	14.918	10.707	10.073	8.857	1.114	4.217	15.084	34.890	178.431	

[a] Enumeration of the models is given in Table 1.

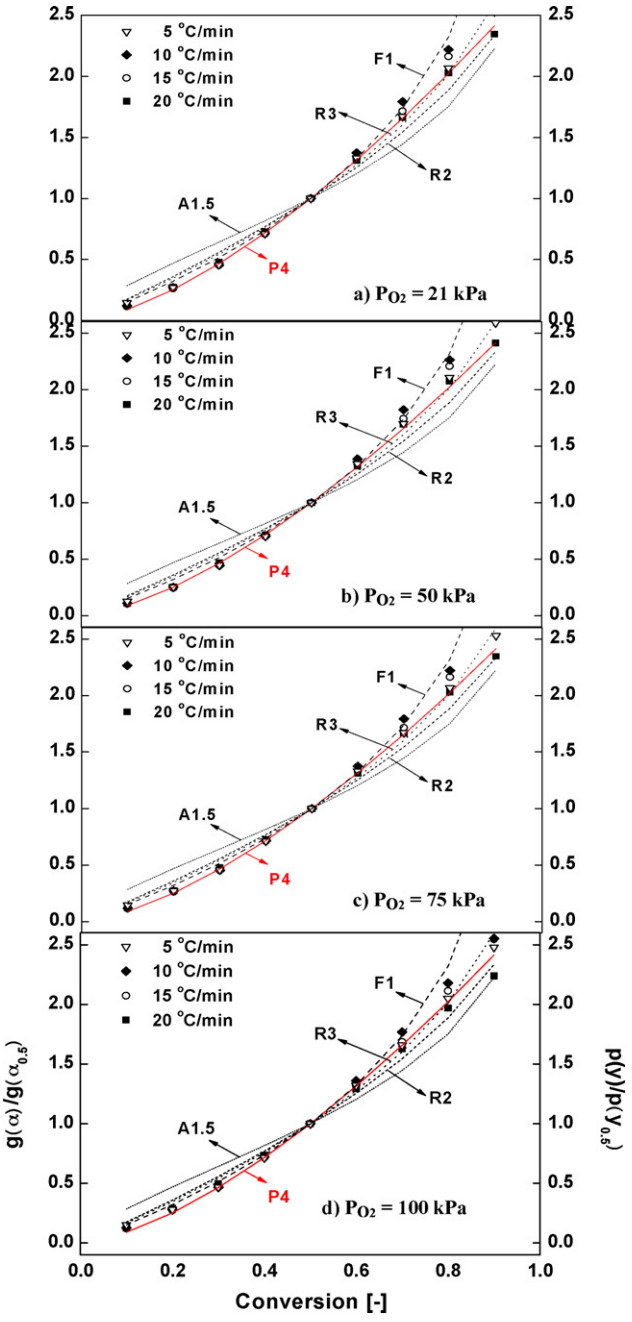

Fig. 8. Master plots of theoretical $g(\alpha)/g(\alpha_{0.5})$ against α for various reaction models (solid lines, as enumerated in Table 1) and experimental values of $p(y)/p(0.5)$ for different O_2 conditions (symbols).

4.4. Evaluation of the oxygen power dependency and pre-exponential factor

By introducing the deribed reaction model, $g(\alpha) = \alpha^{3/2}$, into Eq. (3), Eq. (14) is obtained.

$$\alpha^{3/2} = \frac{ZE}{BR}p(y) \tag{14}$$

The plots of $g(\alpha)$ against $(E/BR)p(y)$ for all the different conditions are constructed in Fig. 9. By using Eq. (12), the Z values were determined from the slopes of the fitted lines shown in

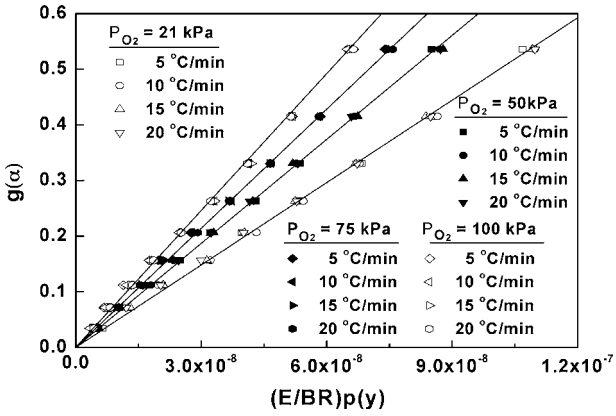

Fig. 9. Determination of Z values by plotting $g(\alpha)$ against $(E/BR)p(y)$ for different O_2 conditions.

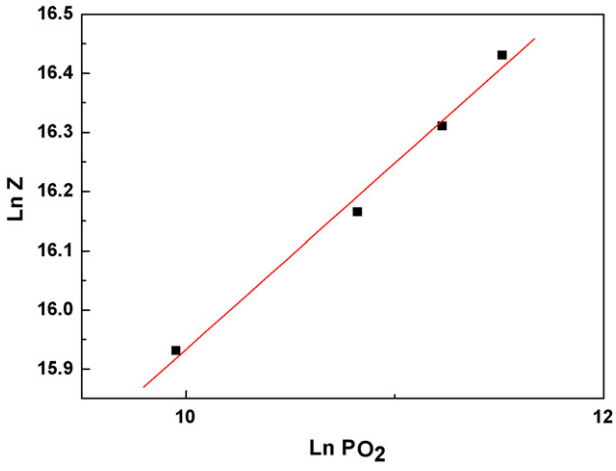

Fig. 10. Determination of pre-exponential factor k_0 and oxygen power dependency n from the slopes of the plots $\ln Z$ against $\ln P_{O_2}$.

Table 3
Determined kinetic parameters of the conversion of NdOCl into Nd_2O_3

Reaction model	$g(\alpha) = \alpha^{3/2}$
Activation energy E (kJ mol^{-1})	228.3 ± 6.1
Pre-exponential factor k_0 (s^{-1} Pa$^{-0.315}$)	3.55×10^5
Power dependence of oxygen n	0.315

Fig. 9. From the averaged Z values for the corresponding oxygen partial pressures, the plots of !!ln Z against ln P_{O_2} were constructed and the results are shown in Fig. 10. The oxygen power dependency n and the pre-exponential factor k_0 were determined by using Eq. (11) and the slope and the intercept of the linearly fitted line in Fig. 10. The slope (n) and the intercept ($\ln k_0$) of the fitted line were determined as 0.315 and 12.78, respectively. Determined kinetic parameters of Eq. (13) are listed in Table 3.

5. Conclusion

The kinetics of the thermal dechlorination and oxidation of NdOCl powder originating from a molten salt process could be established by using non-isothermal TG analyses under various oxygen partial pressures. The conversion of NdOCl into Nd_2O_3

at high temperatures appeared to be an oxygen-dependent endothermic and one-step reaction. The observed activation energy of the reaction was determined as $228.3 \pm 6.1\,\mathrm{kJ\,mol^{-1}}$. A kinetic rate equation was derived for the conversion of NdOCl powder with a power law model ($g(\alpha) = \alpha^{3/2}$). The oxygen power dependency and the pre-exponential factor were determined as 0.315 and $3.55 \times 10^5\,\mathrm{s^{-1}\,Pa^{-0.315}}$, respectively.

Acknowledgement

This study has been carried out under the Nuclear R&D Program by the Korean Ministry of Science and Technology.

References

[1] M. Zawadzki, L. Kepinski, J. Alloys Compd. 380 (2004) 255.
[2] A.G. Dedov, A.S. Loktev, I.I. Moiseev, A. Aboukais, J.F. Lamonier, I.N. Filimonov, Appl. Catal. A: Gen. 245 (2003) 245.
[3] F.B. Noronha, D.A.G. Aranda, A.P. Ordine, M. Schmal, Catal. Today 57 (2000) 275.
[4] Y. Ozawa, Y. Tochihara, A. Watanabe, M. Nagai, S. Omi, Chem. Lett. 32 (2003) 246.
[5] H. Konishi, T. Nohira, Y. Ito, Electrochim. Acta 48 (2003) 563.
[6] H. Konishi, T. Nishikiori, T. Nohira, Y. Ito, Electrochim. Acta 48 (2003) 1403.
[7] S.A. Kuznetsov, M. Gaune-Escard, Electrochim. Acta 46 (2001) 1101.
[8] Y. Yamamura, I. Wu, H. Zhu, M. Endo, N. Asao, M. Mohamend, Y. Sato, Molten Salt Chem. Technol. 5 (1998) 355.
[9] M. Ginic-Markovic, N.R. Choudhury, J.G. Matisons, D.R.G. Williams, J. Thermal. Anal. Calorim. 59 (2006) 409.
[10] N. Shamara, A.K. Sood, S.S. Bhatt, S.C. Chaudhry, J. Thermal. Anal. Calorim. 61 (2000) 779.
[11] B. Saha, A.K. Maiti, A.K. Ghoshal, Thermochim. Acta 444 (2006) 46.
[12] M.A. Gabal, Thermochim. Acta 412 (2006) 55.
[13] C.D. Doyle, J. Appl. Poly. Sci. 4 (1962) 639.
[14] R.C. Everon, H.W.J.P. Neomagus, D. Njapha, Fuel 85 (2006) 418.
[15] E. Sima-Ella, G. Yuan, T. Mays, Fuel 84 (2005) 1920.
[16] T. Wanjun, L. Yuwen, Z. Hen, W. Zhiyong, W. Cunxin, J. Thermal. Anal. Calorim. 74 (2003) 309.
[17] F.J. Gotor, J.M. Criado, J. Málek, N. Koga, J. Phys. Chem. A 104 (2000) 10777.
[18] S. Vyazovkin, C.A. Wight, Thermochim. Acta 340/341 (1999) 53.
[19] T. Wanjun, C. Donghua, AIChE J. 52 (2006) 2211.